Simulation of Sea-ice Thermodynamics by a Smoothed Particle Hydrodynamics Method

Ryszard Staroszczyk

Institute of Hydro-Engineering, Polish Academy of Sciences, ul. Kościerska 7, 80-328 Gdańsk, Poland,
e-mail: rstar@ibwpan.gda.pl

Abstract

The paper deals with the problem of sea-ice pack motion and deformation under the action of wind and water drag forces. Differential equations describing the behaviour of ice, with its very distinct material responses in converging and diverging flows, express the mass and linear momentum balances on a horizontal plane (the free surface of the ocean). The thermodynamic effects (ice melting and lead water freezing) are accounted for by adding source terms to the equations describing the evolution of the ice thickness and area fraction (concentration). These thermodynamic source terms are described by means of a single function that idealizes typical ice growth-rates observed in winter in the Arctic. The equations governing the problem are solved by a fully Lagrangian method of the smoothed particle hydrodynamics (SPH). Assuming that the ice behaviour can be approximated by a non-linearly viscous rheology, the proposed SPH model was used to simulate the flow of a sea-ice pack driven by wind drag stresses and varying seasonal temperatures. The results of numerical simulations illustrate the evolution of an ice pack, including distributions of ice thickness and ice area fraction in space and time for assumed temperature distributions.

List of symbols

a	–	reference particle label,
A, A_0	–	ice concentration (ice area fraction),
A_f	–	critical ice concentration,
b	–	neighbouring particle label,
C_a, C_w	–	dimensionless wind and water drag coefficients,
d	–	initial inter-particle spacing,
$\boldsymbol{D}$	–	strain-rate tensor,
$f(A)$	–	ice – ice contact length function,
$G(h)$	–	ice growth-rate function,
h, h_0	–	ice thickness,

$H(\cdot)$	–	Heaviside unit step function,
$\boldsymbol{I}$	–	unit tensor,
$\boldsymbol{k}$	–	upward vertical unit vector,
K	–	ice strength-compactness parameter,
m	–	mass,
$\boldsymbol{N}$	–	depth-integrated horizontal stress tensor,
p	–	pressure,
R	–	smoothing kernel support radius,
S_A, S_h	–	ice area fraction and thickness growth-rates,
t	–	time,
T, T_m	–	temperature, melting temperature,
$\boldsymbol{u}_a, \boldsymbol{u}_w$	–	wind and water current velocity vectors,
$\boldsymbol{v}$	–	ice velocity vector,
W	–	SPH smoothing kernel function,
$x_i \ (i = 1, 2)$	–	spatial Cartesian co-ordinates,
$\boldsymbol{x}$	–	position vector,
$\alpha(A)$	–	ice ridging function,
γ	–	shear-rate invariant,
ζ	–	ice bulk viscosity,
η	–	ice horizontal dilatation-rate,
μ	–	ice shear viscosity,
ρ	–	ice density,
ρ_a, ρ_w	–	air and water densities,
$\boldsymbol{\sigma}$	–	Cauchy stress tensor,
$\boldsymbol{\tau}_a, \boldsymbol{\tau}_w$	–	wind stress and water drag surface tractions,
ϕ_1, ϕ_2	–	material viscous response functions.

1. Introduction

A typical large sea-ice pack is a complex thermodynamic system comprising a multitude of floes of different size and geometry, driven by wind and water drag stresses, and subject to surface and basal freezing and melting in response to current local mechanical and thermal forcing. As individual floes move about and interact, in either ductile or (much more often) brittle manner, they break, merge and raft on one another, giving rise to large variations in the local ice thickness and ice area fraction (concentration). Since a broken ice cover cannot carry tensile stresses, the mechanical behaviour of an ice pack in converging flow is remarkably different from that in diverging flow. One consequence of this is the development and subsequent propagation of interfaces that separate converging and diverging regions in sea ice, often leading to the fragmentation of an initially coherent pack domain. An important feature of ice is also a significant change in the planar geometry of a domain occupied by the pack, associated with large displacements of boundaries between the coherent ice and the

open sea. All these physical mechanisms, which are difficult to treat both mathematically and numerically, significantly increase the complexity of numerical algorithms and the cost of calculations.

Theoretical descriptions of the behaviour of sea ice are usually based on the assumption that the ice cover can be treated as a two-dimensional continuum moving and deforming on the ocean surface (Hibler 1979, Gray and Morland 1994). Hence, the equations governing the thermodynamic behaviour of sea ice are derived by applying the methods of continuum mechanics. These equations are conventionally solved by applying standard numerical approaches, such as finite-difference or finite-element methods, which use computational grids or meshes on which discrete variables are defined (Hibler 1979, Parkinson and Washington 1979, Flato and Hibler 1992, Hunke and Dukowicz 1997, Schulkes et al 1998, Morland and Staroszczyk 1998). In these discrete techniques, the sea ice dynamics equations are typically solved in the spatial (Eulerian) coordinates. The numerical difficulties associated with the presence of convective terms in the momentum equations, as well as the need to accurately track the position of moving boundaries between the ice and the open sea, make the application of the standard mesh-based methods computationally expensive. It is more natural to solve problems involving large deformations and displacements of boundaries by employing a Lagrangian approach, in which all equations are formulated in the material coordinates. One of such fully Lagrangian approaches is the Smoothed Particle Hydrodynamics (SPH) method, which belongs to the class of meshless discrete techniques. Although the SPH method has already been successfully employed to solve a wide variety of problems encountered in physics and engineering (Monaghan 2005, 2012), its application to the problems involving sea ice is surprisingly very rare (Gutfraind and Savage 1997a, 1997b, 1998), despite the fast development and growing popularity of this method over the past two decades.

The SPH model presented in this work is an extension of a model developed earlier (Staroszczyk 2017) for simulating the behaviour of sea ice without any thermodynamic effects involved. The model is used to simulate the evolution of an ice pack driven by wind stresses and subject to the mechanism of ice growth/decay due to the phase changes (freezing of water and melting of ice). The thermodynamic processes causing the changes in ice mass are modelled here in a simplified manner, expressing ice growth-rates by a single function of only one argument (current ice thickness). This function approximates sea-ice behaviour observed under real Arctic conditions on seasonal time scales (Hibler 1979, Thorndike et al 1975). In this way, some complex (and important) phenomena, such as the effect of brine content and its evolution in sea ice (Bitz and Lipscomb 199l), are ignored. The main objective of this first thermodynamic SPH model, however, is to test how well it performs in simple flow configurations and for simple temperature scenarios, before attempting to construct a fully developed model for more realistic weather-driven ice pack flow simulations. Also for simplicity, the rheological model implemented for describing the ice response to stress is that of a Reiner-Rivlin viscous fluid. In spite of this simplification, the

model captures the major feature of sea-ice behaviour, namely the occurrence of zero tensile stresses in diverging ice flows, as will be seen in the next section.

The paper is structured as follows. First, sea-ice thermodynamics equations, which include the ice mass conservation, the heat energy conservation and the linear momentum balances, are formulated in Section 2. Then, in Section 3, constitutive relations describing the non-linearly viscous behaviour of ice are presented. This is followed by Section 4 in which the discrete SPH model is formulated. The results of numerical simulations by the SPH model are discussed in Section 5. Finally, some conclusions are drawn in the last Section 6.

2. Sea-ice Thermodynamics Equations

A typical sea-ice pack consists of a multitude of individual ice floes, varying in horizontal size and thickness, and of interspersed leads of water, see Fig 3. It can be assumed that the thickness of ice is small compared to a characteristic floe diameter, and that the latter is much smaller than the planar size of the whole pack. Therefore, an ice pack can be regarded as a continuum on macroscopic horizontal scales of tens, hundreds or more kilometres, with the local properties defined by the ice thickness and the ice area fraction, both treated as continuous functions. Hence, the equations governing the thermodynamics of ice can be derived by applying standard methods of continuum mechanics. An example of such an approach is the theory proposed by (Gray and Morland 1994), in which a two-dimensional horizontal formulation for sea ice is developed using the methods and results known from the theory of mixtures. The theoretical results obtained by (Gray and Morland 1994) are used in the present work to construct a discrete SPH model for a sea-ice pack.
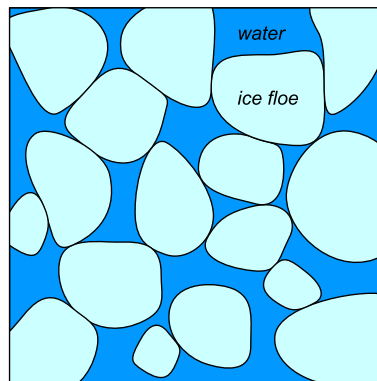
Fig. 1. Horizontal view of a sea-ice pack

Ice pack behaviour is analysed in rectangular Cartesian coordinates, with origin O and the two coordinate axes, x_1 and x_2, placed on a horizontal plane defined by

the mean sea level; for simplicity, the curvature of Earth's surface is neglected. Let t denote time, then the current position of an ice particle on the horizontal plane is defined by the position vector $\boldsymbol{x}(t)$, with components $x_i(t)$, $i = 1, 2$. The motion of the ice pack on the horizontal plane is described by the velocity vector $\boldsymbol{v}(t)$, with components v_1 and v_2. It is assumed that lead water (the water in open spaces between floes) moves horizontally with the same velocity as the local ice field. The pack has a local thickness defined by the function $h(\boldsymbol{x}, t)$. The latter is supposed to be a smooth function of $\boldsymbol{x}$, which is achieved by continuous extension of adjacent ice floe top and bottom surfaces at locations where there is lead water, as illustrated in Figure 2. In general, ice floes occupy only a certain fraction of the total surface of the ice–water system. This ice area fraction, denoted by the function $A(\boldsymbol{x}, t)$, is referred to as the ice concentration; obviously, this function has the property $0 \leq A \leq 1$.
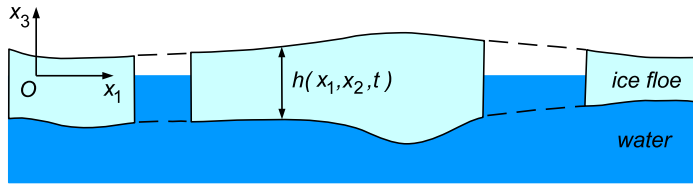

Fig. 2. Vertical cross-section through a sea-ice pack layer

2.1. Mass and Energy Conservation Equations

The mass conservation balance for the ice pack is expressed in terms of two equations, describing the evolution of the local ice thickness h and the local ice concentration A. These two equations are adopted in the following forms (Gray and Morland 1994, Morland and Staroszczyk l998):

$$\frac{DA}{Dt} + A\eta \left[1 - \alpha(A)H(-\eta)\right] = \frac{k}{\rho}, \tag{1}$$

$$\frac{Dh}{Dt} + h\eta\alpha(A)H(-\eta) = q_a + q_w. \tag{2}$$

In the above equations, D/Dt denotes the material (convected) time derivative, and ρ is the intrinsic ice density, with a value of $\rho = 917 \text{ kg m}^{-3}$. The quantity $\eta(\boldsymbol{x}, t)$ is the horizontal dilatation-rate, defined as the divergence of the horizontal velocity field of the ice pack:

$$\eta = \nabla \cdot \boldsymbol{v} = \frac{\partial v_1}{\partial x_1} + \frac{\partial v_2}{\partial x_2}, \tag{3}$$

with the properties

$$\eta \begin{cases} < 0 & \text{in converging flow,} \\ > 0 & \text{in diverging flow.} \end{cases} \tag{4}$$

In equation (3), ∇ denotes the nabla differential operator. The function $H(\cdot)$ in equations (1) and (2) denotes the Heaviside unit step function. By definition,

$$H(-\eta) = \begin{cases} 1 & \text{for} \quad \eta < 0, \quad \text{i.e. in converging flow,} \\ 0 & \text{for} \quad \eta > 0, \quad \text{i.e. in diverging flow.} \end{cases} \tag{5}$$

The Heaviside function is used to describe a very distinct sea-ice pack behaviour, depending on whether the ice is in diverging ($\eta > 0$), or in converging ($\eta < 0$) flow. In the former case, of $\eta > 0$, interactions between individual floes are rare, or completely absent, so stresses between neighbouring floes are small or zero, whereas in the latter case, of $\eta < 0$, interactions between floes are frequent or constant, and the corresponding interaction stresses are significant.

Important physical processes that occur in a converging flow of ice, when individual ice floes collide, are the mechanisms of ice rafting and ridging (Babko et al 2002). In the case of ice rafting, colliding floes override one another, whereas the other mechanism is due to ice crushing and the subsequent piling up of ice rubble on the surfaces of colliding floes. Both mechanisms result in an increase in the local ice thickness and can be regarded as irreversible phenomena. To incorporate these two, in a way similar, processes into a formal description of ice pack behaviour, a single ridging function, denoted here by $\alpha(A)$, is introduced (Hibler 1979). Gray and Morland (1994) postulated that a properly constructed ridging function should necessarily satisfy the conditions

$$\eta \geq 0 : \quad \alpha = 0; \quad \eta < 0 : \quad 0 \leq \alpha \leq 1; \quad \alpha \to 1 \quad \text{as} \quad A \to 1. \tag{6}$$

The following form of this function (Staroszczyk 2017) is adopted in the present work:

$$\alpha(A) = \begin{cases} -2\left(\dfrac{A - A_f}{1 - A_f}\right)^3 + 3\left(\dfrac{A - A_f}{1 - A_f}\right)^2, & \text{for} \quad 0 < A_f < A \leq 1, \\ 0, & \text{for} \quad 0 \leq A \leq A_f. \end{cases} \tag{7}$$

The above cubic form slightly improves on a piecewise linear function proposed by Morland and Staroszczyk (l998). In (7), A_f denotes a critical ice concentration level, below which no ice ridging occurs (despite the converging flow regime), and above which $\alpha(A)$ increases continuously to approach the unit limit as A approaches unity. Two particular values of $A_f = 0.5$ and $A_f = 0.75$ were used in previous numerical simulations carried out by Gray and Morland (1994) and Morland and Staroszczyk (l998).

The right-hand side terms k, q_a and q_w in equations (1) and (2) represent thermodynamic effects on the ice mass balance. The quantity k denotes the mass transfer per unit pack volume per unit time into the ice due to water freezing at vertical floe edges. The terms q_a and q_w, in turn, are the volume fluxes of ice per unit horizontal section into the top ice floe surface ($q_a < 0$ if melting) and out of the bottom surface ($q_w < 0$ if freezing).

The values of the above three mass transfer parameters, k, q_a and q_w, can be determined from an energy balance. In contrast to the purely mechanical behaviour of ice which can be analysed by treating all relevant fields as two-dimensional in the horizontal plane, the energy balance requires the inclusion of vertical temperature gradients through the ice pack thickness. Hence, a three-dimensional temperature field, $T(x_1, x_2, x_3, t)$, must be considered, with x_3 being an upward vertical coordinate axis. Since, under typical ice pack conditions, temperature gradient components in the lateral x_1- and x_2-directions are smaller by several orders of magnitude than those in the vertical x_3-direction, the former gradients can be ignored in a full energy balance (Gray and Morland 1994), which yields a reduced energy balance equation (Morland and Staroszczyk l998) expressed by:

$$\frac{DT}{Dt} = \frac{\kappa}{\rho C} \frac{\partial^2 T}{\partial x_3^2} + \frac{kL}{2\rho AC} + \frac{r_a}{\rho C}. \tag{8}$$

In this equation, κ is the thermal conductivity of ice, C is the specific heat capacity of ice, L is the latent heat of ice melting, and r_a is the radiation deposit per unit volume per unit time.

A full analysis of sea-ice pack behaviour would require a solution of equations (1), (2) and (8) at any given time and location, depending on current thermodynamic conditions which can change very quickly in time and considerably in space. Further, a theoretical description of all thermodynamic phenomena contributing to the local heat budget, and hence to mass fluxes across ice floe surfaces, can be complicated and computationally costly. For these reasons, a simplified approach is followed here, in which the mass transfer terms k, q_a and q_w, all being functions of the spatial horizontal coordinates, time and temperature, are replaced in the mass balance equations (1) and (2) by source terms, S_A and S_h, in a way resembling the approach by Hibler (1979). Hence, the mass balance equations are now re-written in the following forms:

$$\frac{DA}{Dt} + A\eta \left[1 - \alpha(A)H(-\eta)\right] = S_A, \tag{9}$$

$$\frac{Dh}{Dt} + h\eta\alpha(A)H(-\eta) = S_h. \tag{10}$$

The thermodynamic source terms are defined by the relations adapted from Hibler (1979) and expressed as follows:

$$S_h = A\,G\left(\frac{h}{A}\right) + (1 - A)\,G(0), \tag{11}$$

$$S_A = \begin{cases} (1 - A)\,\dfrac{G(0)}{h_0} & \text{for} \quad G(0) > 0, \\ 0 & \text{for} \quad G(0) < 0. \end{cases} \tag{12}$$

The term S_h accounts for the effects of the ice growth or melt on the local ice thickness h. As seen in (11), S_h is expressed as a weighted value of the ice growth-rate over the fraction of the area covered by the ice and the growth-rate of the ice over the area of lead water. The term S_A, in turn, describes how the local mean ice area fraction A changes due to the changes in the local ice thickness. The two separate relations in (12) distinguish between the cases of the ice growth ($G(0) > 0$) and the ice melt ($G(0) < 0$).

A key role in a quantitative description of the source terms S_h and S_A is played by the function $G(h)$, defining the ice growth-rates depending on the current ice thickness h. An exemplary ice growth-rate curve for typical winter conditions in the Arctic Ocean, based on calculations performed by Thorndike et al 1975), was presented by Hibler (1979) in Fig. 3 in his paper. In the present work, two simple analytic forms of the function $G(h)$ are tried to approximate the curve in Hibler's paper for temperatures $T < T_m$ ($G(h) > 0$), where T_m is the ice melting temperature. The case of $T > T_m$ (ice melting, $G(h) < 0$) is not considered here. These two analytic forms are:

$$G_1(h) = G_{\max} \exp\left[-c_1\left(\frac{h}{h_0}\right)\right], \quad \text{with} \quad c_1 = \ln\left(\frac{G_{\max}}{G_0}\right), \tag{13}$$

and

$$G_2(h) = G_{\max} \frac{c_2 h_0}{h + c_2 h_0}, \quad \text{with} \quad c_2 = \frac{G_0}{G_{\max} - G_0}. \tag{14}$$
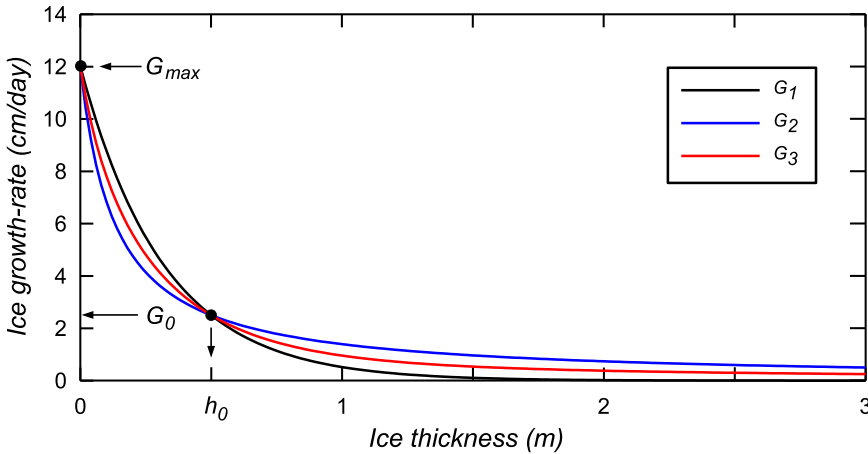
Fig. 3. Ice growth-rate functions $G(h)$ used in simulations. G_0 is the growth-rate at the reference ice thickness h_0, and $G_{\max}$ is the maximum rate at the limit $h \to 0$. The curves G_1 and G_2 are defined by relations (13) and (14) respectively, and $G_3 = (G_1 + G_2)/2$

In the above expressions, the parameter $G_{\max}$ represents the maximum ice growth-rate as the ice thickness $h \to 0$ (that is, when the ice just starts to grow on the lead water), and G_0 is the reference growth-rate occurring at the reference ice thickness h_0; hence,

$G_{\max} = G(0)$ and $G_0 = G(h_0)$. The quantities h_0, G_0 and $G_{\max}$ can be treated as free parameters of the proposed thermodynamic SPH model. Following Hibler (1979), a value of $h_0 = 0.5$ m was adopted, for which (see the plot in Fig. 3 in that paper) $G_0 \approx 2.5$ cm day^{-1}, and $G_{\max} \approx 12$ cm day^{-1}. The plots of the two forms (13) and (14), calculated with these parameters, are presented in Fig. 3. A comparison of the plots of the functions G_1 and G_2 with the growth-rate curve used by Hibler (1979) reveals that the approximation G_1 predicts a too rapid decay of the growth-rate to zero values for large ice thicknesses h, whereas the approximation G_2 gives too large rates for thick ice. For this reason, the mean value of these two functions, that is $G_3 = (G_1 + G_2)/2$, was adopted for numerical simulations as the best fit to the ice growth-rate curve proposed by Hibler (1979).

The ice growth-rate curve presented by Hibler (1979) was obtained for a typical winter temperature in the Arctic – let us denote it by T_0. Hence, the approximations to this curve, given by equations (13) and (14), can also be used only for the characteristic temperature T_0. In order to generalize these approximations to cases (years) in which the average temperature $T \neq T_0$, a temperature-dependent factor $G_T(\bar{T})$ was introduced to scale the ice growth-rate function. The argument $\bar{T}$ of this function is a dimensionless temperature defined by

$$\bar{T} = \frac{T_m - T}{T_m - T_0} \,. \tag{15}$$

By construction, $G_T(\bar{T}) = 1$ for $T = T_0$, and $G_T(\bar{T})$ is a decreasing function of temperature T; that is, the ice growth-rates decrease with increasing temperature T (less ice is produced at higher, but negative, Celsius temperatures). Due to the lack of empirical data, it was arbitrarily assumed in the SPH model calculations that $G_T(\bar{T}) = \bar{T}$ (the scaling factor depends linearly on the seasonal average temperature T, which can be considered as a crude approximation). Hence, the ice growth-rate function used in the simulations had the form

$$G(h, T) = \frac{1}{2} [G_1(h) + G_2(h)] \, \bar{T}, \tag{16}$$

with G_1 and G_2 prescribed by (13) and (14), and $\bar{T}$ defined by (15).

2.2. Linear Momentum Equation

As already stated, it is assumed that the motion of a sea-ice pack is restricted to the horizontal plane Ox_1x_2; that is, the possible motion of ice in the vertical x_3-direction is neglected. The horizontal linear momentum balance equation for the ice pack is derived (Gray and Morland 1994) by integrating full three-dimensional balances through the ice thickness, to yield the expression:

$$\rho h \frac{D\boldsymbol{v}}{Dt} = \nabla \cdot \boldsymbol{N} + \boldsymbol{f}_a + \boldsymbol{f}_w + \boldsymbol{f}_c \,. \tag{17}$$

In the above equation, N, with components N_{11}, N_{12} and N_{22}, is the depth-integrated horizontal stress tensor (with the physical unit Pa · m), f_a and f_w denote external tractions exerted on the top and the bottom surfaces of the ice cover by wind and water drag stress, respectively, and the term f_c represents the Coriolis force effect. On the moderate spatial scales (up to a few hundred kilometres) that will be considered in the further part of this work, the Coriolis effect can be neglected and, therefore, the term f_c will be omitted in all ensuing equations.

The two-dimensional stress N is a mean stress acting on a unit area of the aggregate consisting of ice floes and lead water. By analogy to the theory of two-phase media, it can be interpreted as the so-called partial stress, which is the product of the intrinsic stress in ice, σ, and the ice area fraction, A. Accordingly, N is expressed by

$$N = A\, r(h) f(A)\, \sigma. \tag{18}$$

The stress σ represents the mean value of stress per unit thickness of ice, and it acts when there is full contact between adjacent floes along their edges — such a situation occurs when the ice concentration A is equal to unity (which means that there is no lead water at the interface between adjacent floes). The stress σ will be expressed in terms of the horizontal deformation-rates of the ice pack by a constitutive equation formulated in Section 3.

The definition (18) of the depth-integrated stress includes two proportionality factors, $r(h)$ and $f(A)$. The first factor accounts for the effect of the increasing ice thickness h on the stress N, whereas the second factor, $f(A)$, is the measure of a floe–floe contact length, assumed to increase with increasing ice concentration A. Two common forms (Gray and Morland 1994) of the factor $r(h)$ are a linear dependence on h, and a quadratic function of h. Hence,

$$r(h) = h, \quad \text{or} \quad r(h) = \frac{h^2}{h^*}, \tag{19}$$

where h^* is a typical ice thickness scale. Only the simpler, linear form $r(h) = h$ will be used in numerical simulations. The dimensionless contact length function $f(A)$, necessarily with the properties $f(0) = 0$ and $f(1) = 1$, is adopted in the form

$$f(A) = \frac{\exp[-K(1 - A)] - \exp(-K)}{1 - \exp(-K)}, \quad K \gg 1. \tag{20}$$

It is a slight modification of an earlier formula proposed by Hibler (1979), according to whom the empirical parameter K should have a value of about 20.

The terms f_a and f_w in the motion equation (17) represent tangential tractions acting on the top surface and the base of the ice cover. Similarly to the stress N, these tractions also have the meaning of partial quantities. Hence, they are expressed as products of the intrinsic tractions exerted by wind drag and water currents, denoted by τ_a and τ_b respectively, and of the ice area fraction A. Accordingly, they are defined by the relations

$$f_a = A\tau_a, \quad f_w = A\tau_w. \tag{21}$$

A number of relations expressing the intrinsic surface tractions in terms of the ice, wind and ocean current velocities are known in the literature, including the forms which are linear or quadratic in the velocities. Linear relations were used, among others, by Hibler (1979), Flato and Hibler (1992), Gray nad Morland (1994) and Morland and Staroszczyk (1998). In this work quadratic formulae are adopted, which are expressed in the following forms (Sanderson 1988):

$$\boldsymbol{\tau}_a = C_a \rho_a (\boldsymbol{u}_a - \boldsymbol{v}) |\boldsymbol{u}_a - \boldsymbol{v}|, \quad \boldsymbol{\tau}_w = C_w \rho_w (\boldsymbol{u}_w - \boldsymbol{v}) |\boldsymbol{u}_w - \boldsymbol{v}|. \tag{22}$$

In these relations, ρ_a and ρ_w are, respectively, the air and water densities (with $\rho_w = 1028$ kg m^{-3} for sea water and $\rho_a = 1.3$ kg m^{-3}), and $\boldsymbol{u}_a$ and $\boldsymbol{u}_w$ are, respectively, the wind and ocean current velocity vectors. The parameters C_a and C_w in formulae (22) denote the dimensionless wind stress and water drag coefficients. The particular values of $C_a = 2 \times 10^{-3}$ and $C_w = 4 \times 10^{-3}$ will be used in numerical simulations presented in Section 5.

On account of the definitions (18), (19) and (21), the momentum equation (17) becomes

$$\rho h \frac{\mathrm{D}\boldsymbol{v}}{\mathrm{D}t} = A h f(A) \nabla \cdot \boldsymbol{\sigma} + A (\boldsymbol{\tau}_a + \boldsymbol{\tau}_w), \tag{23}$$

with the ice surface traction terms $\boldsymbol{\tau}_a$ and $\boldsymbol{\tau}_w$ given by relations (22).

3. Constitutive Description of Sea Ice

In the present work, the mechanical behaviour of sea ice is modelled by applying a non-linearly viscous flow law, based on the Reiner-Rivlin constitutive equation (Chadwick 1999). In general, the Reiner-Rivlin flow law expresses the Cauchy stress in terms of a quadratic function of the strain-rate tensor and its three independent invariants. Here a simpler, linear function of the strain-rate tensor is applied:

$$\boldsymbol{\sigma} = \left[\phi_1(\eta, \gamma) \boldsymbol{I} + \phi_2(\eta, \gamma) \boldsymbol{D} \right] H(-\eta), \tag{24}$$

where $\boldsymbol{I}$ is the two-dimensional unit tensor, $\boldsymbol{D}$ is the two-dimensional strain-rate tensor, and ϕ_1 and ϕ_2 are the material viscous response functions. The Heaviside function term $H(-\eta)$ in (24) is used to set the stress to zero in the diverging flow of the sea-ice pack (so that no tensile stress in the ice is admitted). The strain-rate tensor $\boldsymbol{D}$ has the components

$$D_{ij} = \frac{1}{2} \left(\frac{\partial v_i}{\partial x_j} + \frac{\partial v_j}{\partial x_i} \right) \quad (i, j = 1, 2), \tag{25}$$

and η and γ, the strain-rate invariants of $\boldsymbol{D}$, are given by

$$\eta = \mathrm{tr}\, \boldsymbol{D}, \quad \gamma^2 = \frac{1}{2} \mathrm{tr}\, \hat{\boldsymbol{D}}^2. \tag{26}$$

In the above definition, $\mathrm{tr}(\cdot)$ denotes the trace of a tensor, and $\hat{\boldsymbol{D}}$ is the deviatoric strain-rate tensor given by

$$\hat{\boldsymbol{D}} = \boldsymbol{D} - \frac{1}{2}\eta\boldsymbol{I}. \tag{27}$$

Obviously, the above definition of η is equivalent to that given earlier by relation (3). In strain-rate components, the above two invariants, the dilatation-rate η and the shear-rate invariant γ, are expressed by

$$\eta = D_{11} + D_{22}, \quad \gamma^2 = D_{12}^2 + \frac{1}{4}(D_{11} - D_{22})^2. \tag{28}$$

Similarly to (27), the stress tensor $\boldsymbol{\sigma}$ is also decomposed into its axial and deviatoric parts as follows:

$$\hat{\boldsymbol{\sigma}} = \boldsymbol{\sigma} + p\boldsymbol{I}, \quad p = -\frac{1}{2}\,\mathrm{tr}\,\boldsymbol{\sigma}, \tag{29}$$

where p is the mean pressure in ice.

The two functions ϕ_1 and ϕ_2 entering the general flow law (24) define the viscous response of the medium to strain-rates applied. These two functions can be expressed (Morland and Staroszczyk 1998, Staroszczyk 2005) in terms of conventionally used bulk and shear viscosities, ζ and μ respectively, as follows:

$$p = -\zeta\eta, \quad \hat{\boldsymbol{\sigma}} = 2\mu\hat{\boldsymbol{D}}. \tag{30}$$

In view of the latter definitions, the response functions ϕ_1 and ϕ_2 are expressed by

$$\phi_1 = (\zeta - \mu)\eta, \quad \phi_2 = 2\mu, \tag{31}$$

so the viscous flow law (24) becomes

$$\boldsymbol{\sigma} = [(\zeta - \mu)\eta\boldsymbol{I} + 2\mu\boldsymbol{D}]\,H(-\eta). \tag{32}$$

A reduced version of the above constitutive law, obtained by setting $\zeta = \mu$, implying $\phi_1 = 0$, was used by Schulkes et al (1998). Note that (32) is, in general, a non-linear law, since the viscosities ζ and μ are the functions of the strain-rate invariants η and γ.

The viscous properties of ice are known to be very sensitive to its temperature. A standard approach in ice mechanics is to describe the temperature-dependence of the ice viscosity by means of an Arrhenius-type law, by which the viscosity increases exponentially with decreasing absolute temperature of ice. However, at temperatures close to the melting point, this approach is inappropriate, as indicated by experimental data (Mellor 1980), and therefore a different type of relation is needed. Here a relation proposed by Smith and Morland (1981) is applied, derived by correlation with empirical data. This relation expresses the temperature-dependence of ice viscosity by a scaling factor given by

$$a\left(\hat{T}\right) = 0.68\,\exp\left(12\hat{T}\right) + 0.32\,\exp\left(3\hat{T}\right), \tag{33}$$

where the dimensionless temperature $\hat{T}$ is defined by

$$\hat{T} = \frac{(T - T_m)}{\Delta_T}, \quad \Delta_T = 20\text{K}. \tag{34}$$

The function $a(T)$, with the properties $a(T_m) = 1$ and $a(T) < 1$ for $T < T_m$, is a good approximation for temperatures of up to 60 K below the melting point T_m. The rate factor $a(T)$ scales the ice viscosities by

$$\mu(T) = \frac{\mu(T_m)}{a(T)}, \quad \zeta(T) = \frac{\zeta(T_m)}{a(T)}, \tag{35}$$

where $\mu(T_m)$ and $\zeta(T_m)$ are near-melting point ice viscosities.

4. Smoothed Particle Hydrodynamics Formulation

The major idea of the SPH approach consists in representing a continuum by a collection of discrete material particles, each of which carries, in a fully Lagrangian sense, all information on the local physical properties (mass, velocity, temperature, etc.) of the body under consideration. Since no predefined connections between discrete particles are required in the SPH approach (unlike, for instance, in finite-difference and finite-element methods), this method has a great flexibility in dealing with large deformations, material fragmentation, propagation of discontinuity fronts, etc. In order to approximate field variables in terms of their values given at discrete particles, special interpolating functions, often referred to as smoothing kernels, are applied. Typically, a smoothing kernel has non-zero values only in a small domain, called the kernel support (it usually has the shape of a circle in two-dimensional problems). Detailed descriptions of the SPH method can be found in the literature, for instance in papers by Monaghan (1992, 2005, 2012), the co-inventor of this method, or in the book by Li and Liu (2004).

The values of field variables at any (material or spatial) point $\boldsymbol{x}$ of a continuum are calculated by summations over all particles located within the kernel support centred at that point. Similarly, the spatial derivatives of field functions are evaluated by summation formulae involving spatial derivatives of the smoothing kernel functions. Accordingly, the value of a function f at position $\boldsymbol{x}_a$ is approximated using a kernel function, W, by the formula

$$f_a = f(\boldsymbol{x}_a) = \sum_{b=1}^{N} V_b \, f_b \, W(r_{ab}). \tag{36}$$

In (36), a and b denote particle labels, $f_a = f(\boldsymbol{x}_a)$ is a discrete value of f at particle a, N is the number of discrete particles currently located within the kernel support domain of particle a, V_b is the volume of particle b, and $r_{ab} = |\boldsymbol{x}_{ab}| = |\boldsymbol{x}_a - \boldsymbol{x}_b|$ is the distance between particles a and b.

In order to express differential equations in their discrete SPH forms, one needs approximations of differential operators. In the problem considered in this work, only the approximations of the divergence operators for vector and tensor fields are needed. These approximations are adopted in the forms recommended by Monaghan (1992) and Gray et al (2001):

$$(\nabla \cdot \boldsymbol{f})_a = -\frac{1}{\rho_a} \sum_{b=1}^{N} m_b \, \boldsymbol{f}_{ab} \cdot \nabla_a W_{ab} \tag{37}$$

and

$$(\nabla \cdot \boldsymbol{A})_a = \rho_a \sum_{b=1}^{N} m_b \left(\frac{\boldsymbol{A}_a}{\rho_a^2} + \frac{\boldsymbol{A}_b}{\rho_b^2} \right) \cdot \nabla_a W_{ab} \,. \tag{38}$$

In the above two expressions, $\boldsymbol{f}$ and $\boldsymbol{A}$ denote, respectively, a vector and a two-dimensional tensor fields, ρ_a is the density of particle a, m_b is the mass of particle b, and $\boldsymbol{f}_{ab} = \boldsymbol{f}_a - \boldsymbol{f}_b$. $\nabla_a W_{ab}$ denotes the gradient of the kernel function W centred at particle a and calculated at particle b. This gradient is defined by

$$\nabla_a W_{ab} = \frac{\boldsymbol{x}_{ab}}{r_{ab}} \frac{\partial W(r_{ab})}{\partial r_{ab}} \,. \tag{39}$$

Application of the divergence operator approximations (37) and (38) in the mass conservation balances (9) and (10) and the momentum equation (23) yields

$$\frac{\mathrm{d}A_a}{\mathrm{d}t} = (S_A)_a - A_a \eta_a \left[1 - \alpha(A_a) H(-\eta_a) \right], \tag{40}$$

$$\frac{\mathrm{d}h_a}{\mathrm{d}t} = (S_h)_a - h_a \eta_a \alpha(A_a) H(-\eta_a), \tag{41}$$

$$\frac{\mathrm{d}\boldsymbol{v}_a}{\mathrm{d}t} = \frac{\rho_a}{\rho} A_a f(A_a) \sum_{b=1}^{N} m_b \left(\frac{\boldsymbol{\sigma}_a}{\rho_a^2} + \frac{\boldsymbol{\sigma}_b}{\rho_b^2} \right) \cdot \nabla_a W_{ab} + \frac{A_a}{\rho h_a} (\tau_a + \tau_w)_a \,, \tag{42}$$

with the thermodynamic terms $(S_h)_a$ and $(S_A)_a$ defined by equations (11) and (12). Recall that the stress $\boldsymbol{\sigma}$ is prescribed by the constitutive viscous flow law (32). The horizontal dilatation-rate η, when approximated at particle a, is given by

$$\eta_a = (\nabla \cdot \boldsymbol{v})_a = -\frac{1}{\rho_a} \sum_{b=1}^{N} m_b \, \boldsymbol{v}_{ab} \cdot \nabla_a W_{ab} \,, \tag{43}$$

where $\boldsymbol{v}_{ab} = \boldsymbol{v}_a - \boldsymbol{v}_b$. In addition to relations (40)–(42), in order to track the motion of ice on the sea surface, a trajectory equation also has to be solved for each discrete particle:

$$\frac{\mathrm{d}\boldsymbol{x}_a}{\mathrm{d}t} = \boldsymbol{v}_a \,. \tag{44}$$

It should be noted at this point that there is an important qualitative difference between the intrinsic density of ice, ρ, which is constant in time, and the densities ρ_a and ρ_b of discrete material particles, which vary in time. The latter densities connect discrete particle masses m_a (which, in general, change in time due to the mass fluxes described by the terms S_A and S_h) with discrete particle volumes V_a (which change in time due to ice pack deformation) through the equation

$$m_a = \rho_a V_a . \tag{45}$$

The particle density ρ_a, in turn, is related to the local ice concentration A_a and the local ice thickness h_a by the formula

$$\rho_a = \rho A_a h_a . \tag{46}$$

Thus, the particle density ρ_a expresses the mass of ice per unit surface of the sea, so that it has the meaning of a partial density and the physical unit $\mathrm{kg\,m^{-2}}$.

The system of equations (40)–(42) and (44) for particle a is equivalent to six scalar relations for six unknown field functions: A, h, two components of the velocity vector $\boldsymbol{v}$, and two components of the position vector $\boldsymbol{x}$. This system of six equations was integrated in the time domain by a predictor-corrector method (Staroszczyk 2010, 2011). In the calculations, the kernel function W was adopted in the form of a quintic spline function proposed by Morris (1996). As in an earlier paper by Staroszczyk (2017), the standard smoothing kernels W were modified by following an approach proposed by Belytschko et al (1998). This approach makes it possible to better approximate the field variables at discrete particles located close to the open sea boundaries, so that the current positions of these moving boundaries are traced more accurately.

5. Numerical Simulations

In the previous paper (Staroszczyk 2017) the proposed SPH model was applied to simulate the purely mechanical behaviour of an sea-ice pack; that is, the mass conservation equations (9) and (10) were solved without the thermodynamic source terms. In the present paper we first investigate the evolution of the ice thickness and ice concentration in a motionless pack (wind and water drag stresses are zero), in which the ice is subjected only to the action of a temperature field. Hence, in fact, only the mass balance equations are solved at this first stage, before a fully thermodynamic problem for a wind-driven ice pack is solved at the second stage of simulations.

The SPH simulations were carried for a simple, initially rectangular ice pack configuration depicted in Fig. 4, in which the ice is constrained by three solid boundaries, and has only one ice–open sea boundary. The ice pack had the initial horizontal dimensions of $600\,\mathrm{km} \times 600\,\mathrm{km}$. The corresponding SPH model, with the initial grid of particles shown in Fig. 4, consisted of $60 \times 60 = 3600$ particles uniformly distributed along both coordinate axes, with an inter-particle spacing of 10 km (the colours of the particles have no physical meaning and are used entirely for illustration purposes). The
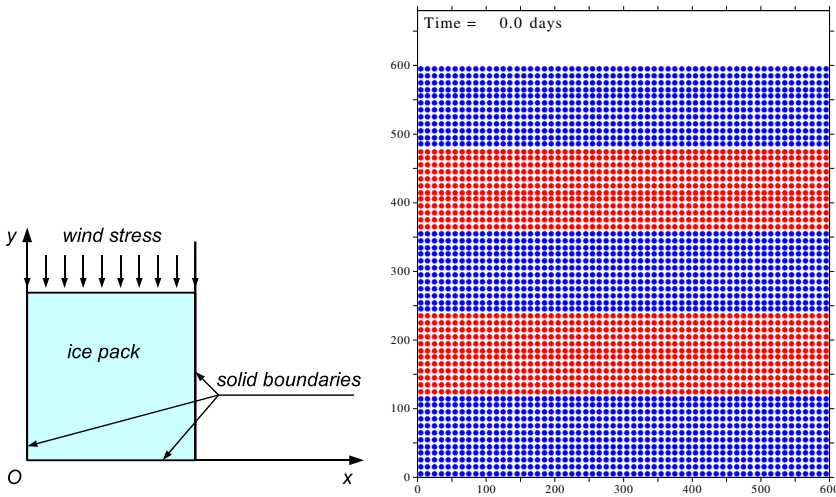
Fig. 4. Simple ice pack flow configurations used in numerical simulations and the initial grid of discrete particles
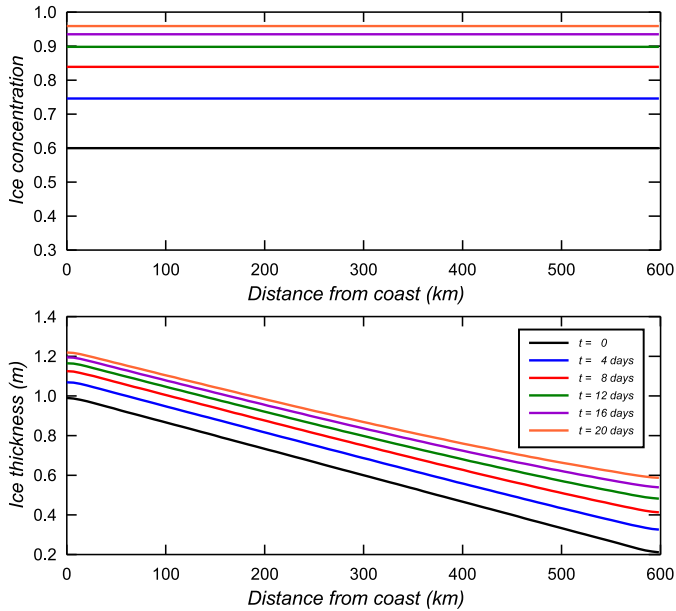
initial ice thickness and concentration distributions were assumed to vary in a linear manner along one (x or y) coordinate axis. Also, the simple air temperature fields $T(x, y, t)$ were adopted, with T being either uniform in space or linearly varying along one of the two coordinate axes, and remaining constant in time throughout the simulations. In all the simulations, the ice growth-rate function parameters (see Fig. 3) were as follows: $G_{max} = 12$ cm day^{-1}, $G_0 = 2.5$ cm day^{-1}, $h_0 = 0.5$ m, and the reference temperature was $T_0 = -40°$.

The following Figures 5, 6 and 7 show the evolution of the ice concentration A and ice thickness h for three one-dimensional cases involving different combinations of the initial distributions of A and h. In all three cases the air temperature was assumed as $T = -20°$. In the first case, illustrated by the plots in Fig. 5, the ice had initially the thickness $h = 1$ m and the ice concentration varied between $A = 0.8$ at the coast $y = 0$ to $A = 0.4$ at the open sea edge at $y = 600$ km. The plots show how the distributions of A and h change due to the freezing of lead water and ice during a period of 20 days. It is seen that the largest increase in both ice concentration and ice thickness takes place in regions in which the initial ice concentration was smallest (that is, in regions where the area fraction occupied by lead water is largest, and hence the growth of ice due to water freezing is most intense).

In the case illustrated in Fig. 6, the initial ice concentration was assumed constant and equal to $A = 0.6$, while the ice thickness varied linearly from $h = 1$ m at the coast $y = 0$ to $h = 0.2$ m at the ice pack edge at $y = 600$ km. One can see that in this case the ice concentration remains uniform throughout the ice pack at all times, irrespective of the current local ice thickness. Obviously, this feature is a consequence of the adopted form of the mass balance, expressed by the first term in equation (12), in which the thermodynamic term S_A does not depend on h and S_h.
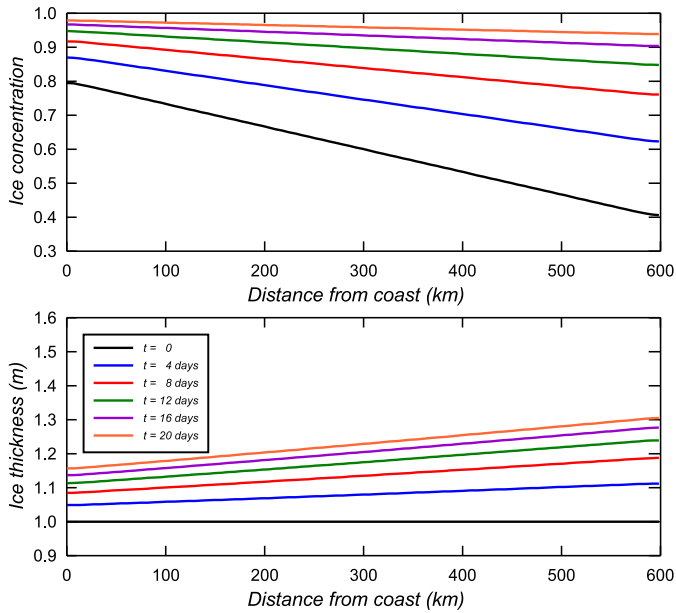
Fig. 5. Evolution of ice concentration and ice thickness profiles along the y-axis for the ice pack configuration shown in Fig. 4a, for an initially uniform ice thickness of 1 m and a linearly varying ice concentration (air temperature $T = -20°$). The same labelling applies to both plots

Fig. 6. Evolution of ice concentration and ice thickness profiles along the y-axis for the ice pack configuration shown in Fig. 4a, for an initially uniform ice concentration of 0.6 and a linearly varying ice thickness (air temperature $T = -20°$). The same labelling applies to both plots
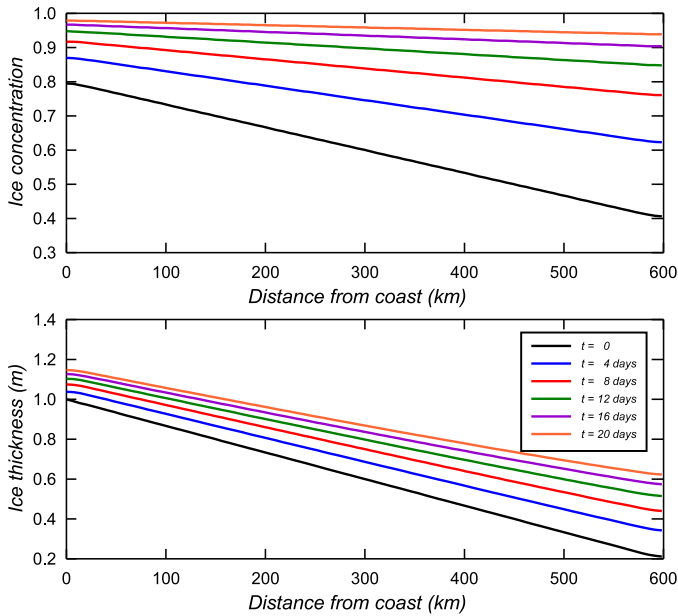
Fig. 7. Evolution of ice concentration and ice thickness profiles along the y-axis for the ice pack configuration shown in Fig. 4a, for initially linearly varying ice concentration of 0.6 and ice thickness distributions (air temperature $T = -20°$). The same labelling applies to both plots

The plots in Fig. 7 illustrate a case in which both the initial ice concentration and ice thickness vary linearly with the distance y from the coastline. There is no much difference between the results in this figure and the corresponding plots in Fig. 5a and Fig. 6b is observed.

In order to investigate a more realistic problem in which a sea-ice pack is both deformed in the horizontal plane due to wind drag stresses and undergoes ice mass changes due to thermodynamic effects (that is, full thermodynamic equations (9) and (10) are solved), a flow configuration depicted in Fig. 8 was considered. In this flow configuration, the ice pack initially occupies a rectangular domain $L_1 \times L_2$, with three sides (Γ_1, Γ_2 and Γ_3) of the ice pack domain being constrained by solid boundaries, and the fourth side (Γ_4) being an open sea boundary. It is assumed that the ice is driven by a vortex geostrophic wind field, with the vortex centre, marked by the cross in the figure, located at the open sea at a certain distance from the initial line of the ice pack edge Γ_4. This configuration was chosen for simulations, since it generates both converging and diverging ice flows in the pack domain. Detailed equations describing the wind velocities in the vortex field can be found in papers by Flato (1993), Morland and Staroszczyk (1998) and Staroszczyk (2017). Here we only note that the wind speed is zero at the vortex centre, increases linearly from zero to its maximum value u_0 at some distance R_0 from the vortex centre, and then decreases monotonically to zero with the distance increasing to infinity.
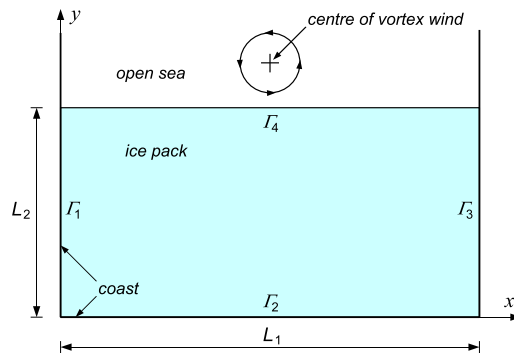
Fig. 8. Rectangular ice pack with three solid boundaries (Γ_1, Γ_2 and Γ_3) and one open water boundary (Γ_4) driven by a vortex wind field, with the vortex centre at the open sea (indicated by the cross)

The numerical simulations were run for an ice pack with dimensions $L_1 = 600$ km and $L_2 = 300$ km and the wind vortex centre situated 50 km off the initial position of the ice pack edge Γ_4. Uniform initial ice thickness and ice concentration were adopted, with $h = 1$ m and $A = 0.6$ at the start of ice pack deformation. The magnitudes of viscosities were $\zeta = 2 \times 10^9$ Pa·s and $\mu = 1 \times 10^9$ Pa·s. A uniform air temperature field $T = -20°$ was adopted in the calculations. The SPH model consisted of $60 \times 30 = 1800$ discrete particles, and was integrated with a time step length of 0.01 hr. Free-slip conditions were assumed along the coastlines Γ_1, Γ_2 and Γ_3.

The results of SPH simulations presented below were obtained for a maximum vortex wind speed $u_0 = 5$ m s^{-1} acting at a distance $R_0 = 40$ km from the vortex centre. The plots in Fig. 9 show the evolution of the ice concentration field $A(x, y, t)$ over a period of 20 days. Compared are the results predicted by the SPH model for the purely mechanical behaviour of ice (the plots on the left) and the full thermodynamical model (the plots on the right). It can be observed that, for the set of parameters used in the simulations, the changes in the ice concentration A are dominated by the thermodynamic effects associated with the freezing of lead water, with A continuously increasing throughout the pack so that the minimum values of A exceed 0.9 everywhere. In contrast, the ice concentrations obtained for a purely mechanical deformation of the pack range from about 0.4 (the decrease from the initial value of 0.6 is due to ice divergence) to about 0.7 (the increase is due to the ice ridging process in converging flow).

The plots in Fig. 10 illustrate changes in the ice thickness h resulting from the horizontal deformation of ice and its growth due to freezing. It is seen that the final ice thickness varies between about 1.3 m and about 1.4 m. On the contrary, changes in the thickness of ice caused solely by its deformation due to the wind action are insignificant (therefore they are not illustrated), since the maximum final values of h do not exceed 1.05 m (a mere 5 cm increase in the ice thickness compared to the initial value of 1 m).
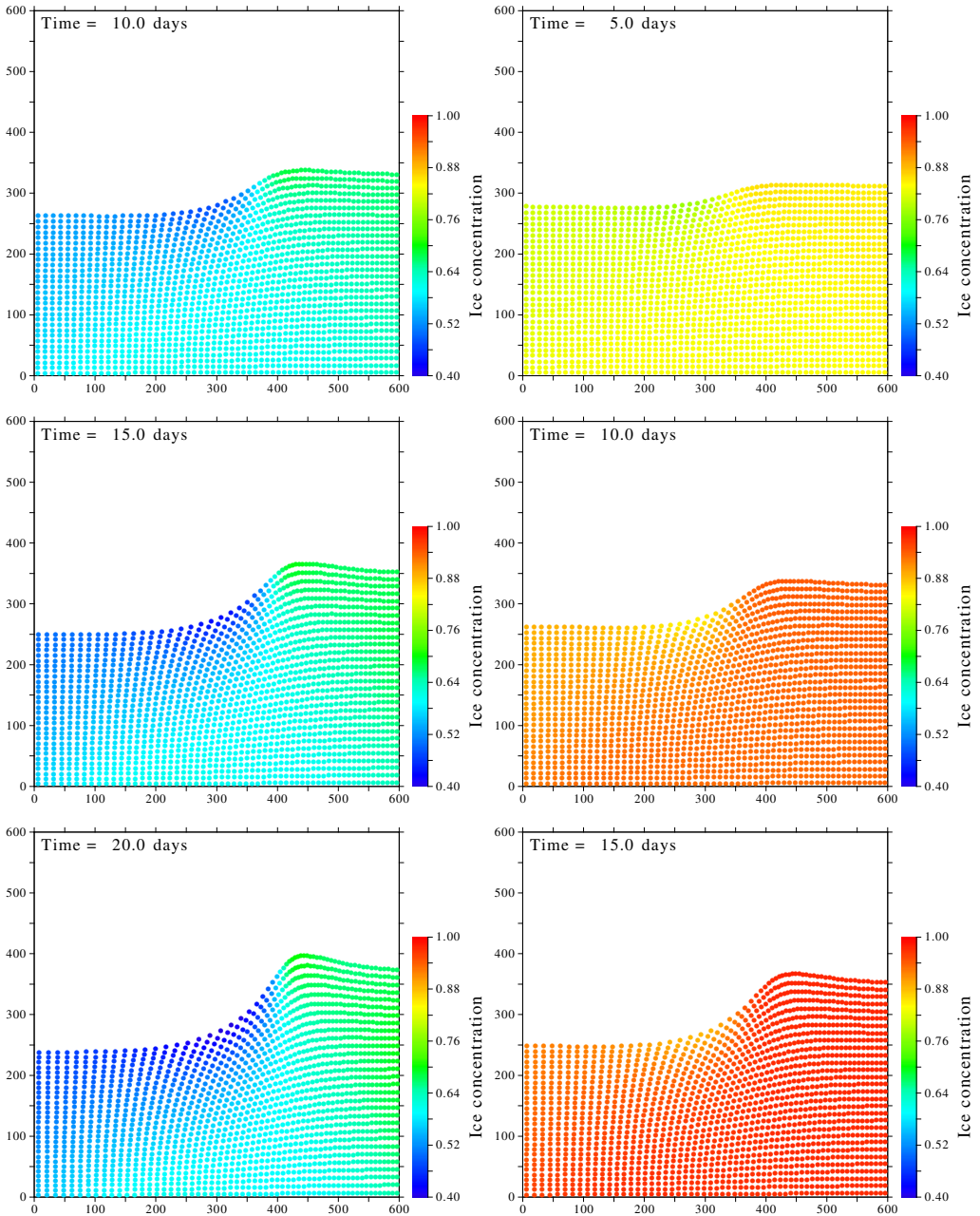
Fig. 9. Evolution of an initially rectangular ice pack shown in Fig. 8 with free-slip conditions along the coastlines. Comparison of ice concentration distributions for the purely mechanical behaviour of ice (plots on the left) and a fully thermodynamic behaviour (plots on the right). The initial concentration was $A = 0.6$
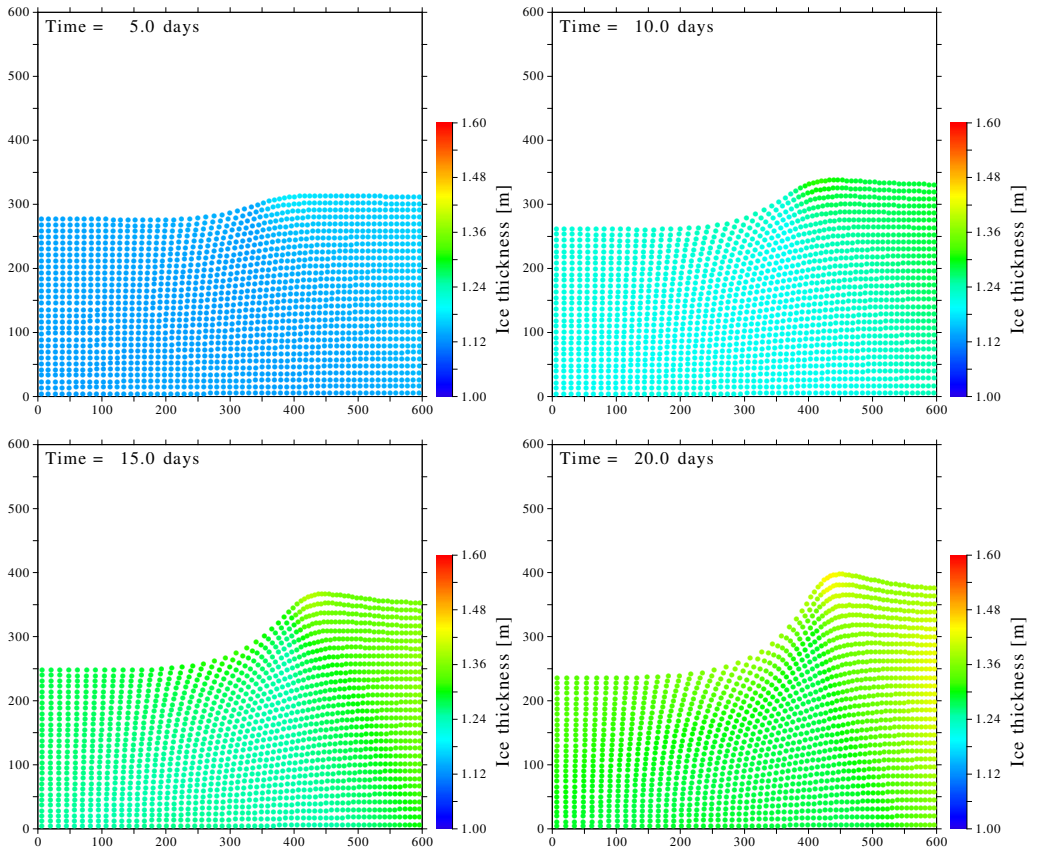
Fig. 10. Evolution of an initially rectangular ice pack shown in Fig. 8 with free-slip conditions along the coastlines. Ice thickness distributions after 5, 10, 15 and 20 days of thermodynamic ice flow. The initial ice thickness was $h = 1.0$ m

6. Conclusions

In this paper, a smoothed particle hydrodynamics model was developed for the purpose of simulating the thermodynamic behaviour of sea ice on geophysical scales. The mechanisms of the growth or decay of the sea-ice cover due to ice melting or lead water freezing were incorporated into the model by adopting a simple approach in which the growth rates of the thickness and concentration of ice depend on a single function that idealizes the observed macroscopic behaviour of ice in the Arctic.

The SPH model was used to simulate the evolution of an ice pack driven by wind and water drag stresses in a prescribed temperature field. The results obtained demonstrate that the SPH approach yields smooth and stable solutions even for relatively long simulation times without the need to introduce artificial dissipation terms in the momentum balance equations (which is often the case in large-scale climate models using conventional mesh methods).

It has been shown (at least for the parameters used in the simulations) that, under typical winter conditions in the Arctic, the evolution of the thickness and concentration of ice is dominated by its thermodynamics, with the effects of its mechanical deformation on the ocean surface playing a minor role.

References

Babko O., Rothrock D. A., Maykut G. A. (2002) Role of rafting in the mechanical redistribution of sea ice thickness, *J. Geophys. Res.*, **107** (C8), 3113, DOI: 10.1029/1999JC000190.

Belytschko T., Krongauz Y., Dolbow J., Gerlach C. (1998) On the completeness of meshfree particle methods, *Int. J. Numer. Meth. Eng.*, **43** (5), 785–819, DOI: 10.1002/(SICI)1097-0207(19981115) 43:5.

Bitz C. M., Lipscomb W. H. (1999) An energy-conserving thermodynamic model for sea ice, *J. Geophys. Res.*, **104** (C7), 15 669–15 677, DOI: 10.1029/1999JC900100.

Chadwick P. (1999) *Continuum Mechanics: Concise Theory and Problems*, Dover, Mineola, New York, 2nd edn.

Flato G. M. (1993) A particle-in-cell sea-ice model, *Atmos.-Ocean*, **31** (3), 339–358.

Flato G. M., Hibler W. D. (1992) Modeling pack ice as a cavitating fluid, *J. Phys. Oceanogr.*, **22** (6), 626–651.

Gray J. M. N. T., Morland L. W. (1994) A two-dimensional model for the dynamics of sea ice, *Phil. Trans. R. Soc. Lond.*, A 347 (1682), 219–290, DOI: 10.1098/rsta.1994.0045.

Gray J. P., Monaghan J. J., Swift R. P. (2001) SPH elastic dynamics, *Comput. Meth. Appl. Mech. Eng.*, **190** (49-50), 6641–6662, DOI: 10.1016/S0045-7825(01)00254-7.

Gutfraind R., Savage S. B. (1997a) Marginal ice zone rheology: Comparison of results from continuum-plastic models and discrete-particle simulations, *J. Geophys. Res.*, **102** (C6), 12 647–12 661, DOI: 10.1029/97JC00124.

Gutfraind R., Savage S. B. (1997b) Smoothed particle hydrodynamics for the simulation of broken-ice fields: Mohr-Coulomb-type and frictional boundary conditions, *J. Comput. Phys.*, **134** (2), 203–215, DOI: 10.1006/jcph.1997.5681.

Gutfraind R., Savage S. B. (1998) Flow of fractured ice through wedge-shaped channels: smoothed particle hydrodynamics and discrete-element simulations, *Mech. Mater.*, **29** (1), 1–17.

Hibler W. D. (1979) A dynamic thermodynamic sea ice model, *J. Phys. Oceanogr.*, **9** (4), 815–846.

Hunke E. C., Dukowicz J. K. (1997) An elastic-viscous-plastic model for sea ice dynamics, *J. Phys. Oceanogr.*, **27** (9), 1849–1867.

Li S., Liu W. K. (2004) *Meshfree Particle Methods*, Springer, Berlin.

Mellor M. (1980) Mechanical properties of polycrystalline ice, [in:] *Physics and Mechanics of Ice, Proc. IUTAM Symp. Copenhagen 1979* (ed. P. Tryde), Springer, Berlin, 217–245.

Monaghan J. J. (1992) Smoothed particle hydrodynamics, *Annu. Rev. Astron. Astrophys.*, **30**, 543–574, DOI: 10.1146/annurev.aa.30.090192.002551.

Monaghan J. J. (2005) Smoothed particle hydrodynamics, *Rep. Prog. Phys.*, **68** (8), 1703–1759, DOI: 10.1088/0034-4885/68/8/R01.

Monaghan J. J. (2012) Smoothed particle hydrodynamics and its diverse applications, *Annu. Rev. Fluid Mech.*, **44**, 323–346, DOI: 10.1146/annurev-fluid-120710-101220.

Morland L. W., Staroszczyk R. (1998) A material coordinate treatment of the sea-ice dynamics equations, *Proc. R. Soc. Lond.*, A **454** (1979), 2819–2857, DOI: 10.1098/rspa.1998.0283.

Morris J. P. (1996) *Analysis of Smoothed Particle Hydrodynamics with Applications*, Ph.D. thesis, Monash University, Melbourne, Australia.

Parkinson C. L., Washington W. M. (1979) A large-scale numerical model of sea-ice, *J. Geophys. Res.*, **84** (C1), 311–337, DOI: 10.1029/JC084iC01p00311.

Sanderson T. J. O. (1988) *Ice Mechanics. Risks to Offshore Structures*, Graham and Trotman, London.

Schulkes R. M. S. M., Morland L. W., Staroszczyk R. (1998) A finite-element treatment of sea ice dynamics for different ice rheologies, *Int. J. Numer. Anal. Meth. Geomech.*, **22** (3), 153–174.

Smith G. D., Morland L. W. (1981) Viscous relations for the steady creep of polycrystalline ice, *Cold Reg. Sci. Technol.*, **5** (2), 141–150.

Staroszczyk R. (2005) Loads exerted by floating ice on a cylindrical structure, *Arch. Hydro-Eng. Environ. Mech.*, **52** (1), 39–58.

Staroszczyk R. (2010) Simulation of dam-break flow by a corrected smoothed particle hydrodynamics method, *Arch. Hydro-Eng. Environ. Mech.*, **57** (1), 61–79.

Staroszczyk R. (2011) Simulation of solitary wave mechanics by a corrected smoothed particle hydrodynamics method, *Arch. Hydro-Eng. Environ. Mech.*, **58** (1-4), 23–45, DOI: 10.2478/v10203-011-0002-9.

Staroszczyk R. (2017) SPH modelling of sea-ice pack dynamics, *Arch. Hydro-Eng. Environ. Mech.*, **64** (2), 115–137, DOI: 10.1515/heem-2017-0008.

Thorndike A. S., Rothrock D. A., Maykut G. A., Colony R. (1975) The thickness distribution of sea ice, *J. Geophys. Res.*, **80**, 4501–4513, DOI: 10.1029/JC080i033p04501.